

Light-induced pitch transitions in photosensitive cholesteric liquid crystals: Effects of anchoring energy

Tetiana N. Orlova,^{1,2,*} Roman I. Iegorov,^{1,3,†} and Alexei D. Kiselev^{1,‡}

¹*Institute of Physics of National Academy of Sciences of Ukraine,
prospekt Nauki 46, 03680 Kiev, Ukraine*

²*LOMA (Laboratoire Ondes et Matiere d'Aquitaine),
University Bordeaux 1, 351 Cours de la Liberation, 33400 Talence, France*

³*UFOLAB (Ultrafast Optics & Lasers Laboratory),
Bilkent University, 06800 Bilkent, Ankara, Turkey*

(Dated: May 11, 2018)

We experimentally study how the cholesteric pitch, P , depends on the equilibrium pitch P_0 in planar liquid crystal (LC) cells with both strong and semistrong anchoring conditions. The cholesteric phase was induced by dissolution in the nematic LC the right-handed chiral dopant 7-dehydrocholesterol (7-DHC, provitamin D_3) which transforms to left-handed tachysterol under the action of uv irradiation at the wavelength of 254 nm. By using the model of photoreaction kinetics we obtain the dependencies of isomer concentrations and, therefore, of the equilibrium pitch on the uv irradiation dose. The cholesteric pitch was measured as a function of irradiation time using the polarimetry method. In this method, the pitch is estimated from the experimental data on the irradiation time dependence of the ellipticity of light transmitted through the LC cells. It is found that the resulting dependence of the twist parameter $2D/P$ (D is the cell thickness) on the free twisting number parameter $2D/P_0$ shows jump-like behavior and agrees well with the known theoretical results for the anchoring potential of Rapini-Papoulier form.

PACS numbers: 61.30.Hn, 64.70.M-, 42.70.Df, 42.70.Gi

Keywords: cholesteric liquid crystal; helix pitch; anchoring energy, polarization of light

I. INTRODUCTION

In equilibrium structures of chiral nematic liquid crystals also known as *cholesteric liquid crystals* (CLC) molecules align on average along a local unit director $\hat{\mathbf{n}}(\mathbf{r})$ that rotates in a helical fashion about a uniform twist axis [1]. This tendency of CLCs to form helical twisting patterns is caused by the presence of anisotropic molecules with no mirror plane — so-called chiral molecules (see [2, 3] for reviews).

In planar CLC cells bounded by two parallel substrates orientational structures (director configurations) are strongly affected by the anchoring conditions at the boundary surfaces. These conditions break the translational symmetry along the twisting axis and, in general, the helical form of the director field will be distorted.

Nevertheless, when the anchoring conditions are planar and out-of-plane deviations of the director are suppressed, it might be expected that the configurations still have the form

* Email address: orlovat@gmail.com

† Email address: rommel.ua@gmail.com

‡ Email address: kiselev@iop.kiev.ua

of the ideal helical structure:

$$\hat{\mathbf{n}} = \cos \phi \hat{\mathbf{x}} + \sin \phi \hat{\mathbf{y}}, \quad \phi = qz + \phi_0, \quad (1)$$

where $q = 2\pi/P$ is the *helix wave number* and ϕ_0 is the phase at $z = 0$. But, by contrast with the case of unbounded CLCs, the helix twist wave number q will now differ from $q_0 = 2\pi/P_0$.

A mismatch between the twist imposed by the boundary conditions and the equilibrium pitch P_0 may produce two metastable twisting states that are degenerate in energy and can be switched either way by applying an electric field [4]. This bistability underlines the mode of operation of bistable liquid crystal devices [5–8].

More generally the metastable twisting states in CLC cells appear as a result of interplay between the bulk and the surface contributions to the free energy. The free twisting number q_0 and the anchoring energy are among the key factors that govern their properties. Specifically, varying q_0 will change the twist wave number of the twisting state, q , and may result in sharp transitions — the so-called *pitch transitions* — between different branches of metastable states. The dependence of the twist wave number q on the free twisting number q_0 is then discontinuous.

In particular, these discontinuities manifest themselves in a jump-like temperature dependence of selective light transmission spectra [9–12]. Different mechanisms behind the temperature variations of the pitch in CLC cells and hysteresis phenomena were discussed in Refs. [13–15]. A comprehensive stability analysis of the helical structures in CLC cells with symmetric and asymmetric boundary conditions was performed in Ref. [16]. The effects of bistable surface anchoring and mechanical strain on the pitch transitions have been studied theoretically in the recent papers [17] and [18], respectively.

In practice, most cholesteric liquid crystals are prepared on the basis of nematic LC mixtures doped with chiral additives that induce a helical structure [19]. For photosensitive chiral dopants, their helical twisting power and thus the equilibrium helix pitch may, in principle, be controlled by light giving rise to the technologically promising effect of phototunable selective reflection (i.e. a change in the spectral position of the bandgap with light exposure) [20–24]. The mechanism underlying the phototunable reflection typically involves photoinduced changes in dopant conformation that affect the LC's helical twisting power (see the recent review [25]).

On the other hand, the light-driven variations of the free twist wave number may trigger the pitch transitions discussed above and can be used as a tool to explore the details of such transitions, depending on a variety of factors. In particular, the surface anchoring energy is known to have a profound effect on the pitch transitions. These surface mediated effects will be of our primary concern.

More specifically, we shall study the pitch transitions in photosensitive CLC cells with strong and semistrong anchoring conditions by using an experimental method that involves modeling of the photoreaction kinetics combined with polarimetry measurements. The results of modeling of the photoreaction kinetics are used to obtain the equilibrium pitch P_0 as a function of the uv irradiation time. A similar irradiation time dependence of the pitch in the CLC cells, P , is extracted from experimental data on the ellipticity of transmitted light measured at different irradiation doses. The resulting dependence of the twist wave number q on the free twisting number q_0 describes the pitch transitions and can be interpreted using known theoretical models.

The paper is organized as follows. Experimental details are given in Sec. II, where we describe the materials and the methods of measurements. In Sec. III, we present the

experimental data and apply the theoretical results [16] to interpret them. Concluding remarks are given in Sec. IV. Technical details on the method used to compute the ellipticity of light transmitted through CLC cells are relegated to Appendix A.

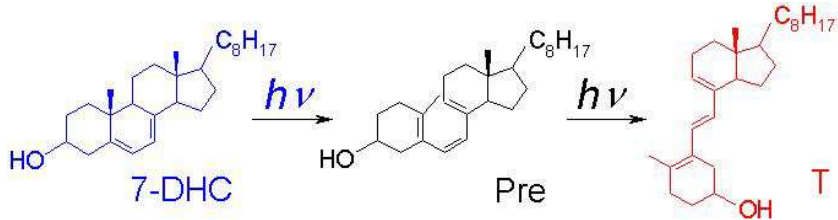


Figure 1: (Color online) Scheme of key 7-DHC phototransformations in a nematic LC matrix under uv irradiation at the wavelength $\lambda_{uv} = 254$ nm (see Refs. [26, 27] for more details). 7-DHC is provitamin D₃, Pre indicates previtamin D, and T stands for tachysterol.

II. EXPERIMENT

In this section we describe the samples and the experimental technique used to estimate both the equilibrium pitch, P_0 , and the pitch characterizing the helical structures formed in the CLC cells. For this purpose, in Sec. II A, the method of uv absorption spectroscopy is used in combination with modeling the kinetics of 7-DHC photoreaction to determine the concentrations of photoisomers that govern the equilibrium pitch. In Sec. II B, we present the experimental results for the ellipticity of light transmitted through the cells that are used to estimate the pitch in the CLC cells.

A. Photokinetics of equilibrium pitch

As a system with light controlled CLC pitch, we have used the nematic MLC-6815 (Merck) doped with the uv-sensitive right-handed chiral dopant provitamin D₃ (7-dehydrocholesterol, 7-DHC) with the helical twisting power $HTP = +3.5 \mu\text{m}^{-1}\text{wt.}^{-1}$. Under the action of uv irradiation this dopant (provitamin D₃) is known to undergo transformation into the left-handed *trans*-isomer tachysterol with $HTP = -8.5 \mu\text{m}^{-1}\text{wt.}^{-1}$ [28]. By contrast, the nematic mixture MLC-6815 is uv-transparent at wavelengths ranged from 240 nm to 400 nm and the liquid crystal host remains stable under such uv irradiation.

The kinetics of the 7-DHC photoreaction is detailed in Refs. [29, 30]. It is well known that, in ethanol solution, the efficiency of 7-DHC conversion to the *trans*-isomer tachysterol under uv irradiation at the wavelength $\lambda_{uv} = 254$ nm is about 60%. This photo-transformation is thermally irreversible and is accompanied by increase of the absorption maximum at the wavelength 282 nm. This increase can be measured using the method of uv absorption spectroscopy and the results can be used for an indirect assessment of the tachysterol concentration.

In nematic LCs, the efficiency of tachysterol accumulation strongly depends on the initial 7-DHC concentration [26–28]. In our experiment, the initial 7-DHC concentration was $C_{7-DHC} \approx 0.4 \text{ wt.}\%$. At this concentration, we have 100% efficiency of 7-DHC conversion to

tachysterol. For this case, the photochemical transformations of 7-DHC are schematically illustrated in Fig. 1. Note that we additionally controlled the photoreaction efficiency by performing measurements of the uv absorption spectra before irradiation and at the time corresponding to maximum increase of absorption at the wavelength 282 nm (it typically takes about 6 min).

For the simplified scheme shown in Fig. 1, the temporal evolution of the photoisomer concentrations can be evaluated using the kinetic model of the 7-DHC photoreaction developed in Ref. [31]. The concentrations computed as a function of the uv irradiation time are shown in Fig. 2(a). The important point is that, in our calculations, the effect of the liquid crystal host on the quantum yields of phototransformations is taken into account.

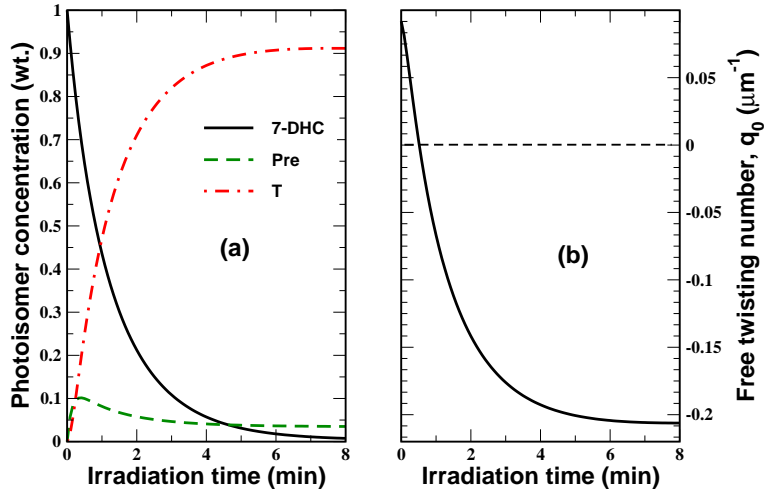


Figure 2: (Color online) (a) Photoisomer concentrations and (b) equilibrium cholesteric wave number $q_0 = 2\pi/P_0$ computed as a function of the irradiation time.

According to the well-known formula

$$P_0^{-1} = \sum_i w_i HTP_i C_i, \quad (2)$$

where w_i is the weight fraction of the i th chiral photoisomer, and the equilibrium cholesteric pitch P_0 is determined by the photoisomer concentrations. The calculated concentrations can now be substituted into Eq. (2) to obtain the irradiation time dependence of the free twisting wave number depicted in Fig. 2(b).

In our experiments, we have used the planar CLC cells of the thickness D varied between 55 μm and 65 μm . At the initial 7-DHC concentration $C_{7-\text{DHC}} \approx 0.4$ wt.%, the photoinduced reorientation processes in such cells are not complicated by inhomogeneity effects related to the formation of highly twisted states.

B. Polarimetry measurements

When a light beam propagates through an optically anisotropic medium, the anisotropy is known to greatly affect its state of polarization [32]. This state is generally described by the Stokes parameters and can be conveniently represented by a polarization ellipse whose

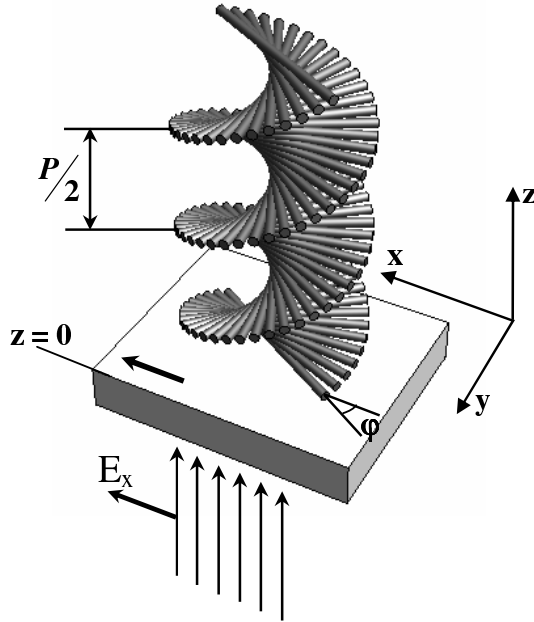


Figure 3: Geometry of normal incidence: A plane wave of linearly polarized light is impinges on the CLC cell.

orientation and eccentricity are specified by the azimuthal angle of polarization (*polarization azimuth*) ϕ_p and the *ellipticity* ϵ_{ell} , respectively [33–35].

For light propagating through a CLC cell where the optical anisotropy is determined by the helical orientational structure (1), its ellipticity is sensitive to the pitch of the CLC spiral [36]. Thus the cholesteric pitch P in photosensitive CLC cells may, in principle, be estimated by measuring the ellipticity of light passed through the cells.

In our experiments, the measurements were performed for light which is normally incident onto the aligned substrate and is linearly polarized along the direction of rubbing. Figure 3 illustrates the geometry of normal incidence.

We have used planar CLC cells where the photosensitive CLC was sandwiched between quartz substrates. In the symmetric case of strong anchoring conditions, both the quartz substrates were coated with rubbed polydimethylsiloxane aligning layers which are insensitive to the uv irradiation. We have also examined asymmetric CLC cells with semistrong anchoring conditions. These cells were assembled using the exiting substrate without the aligning coating.

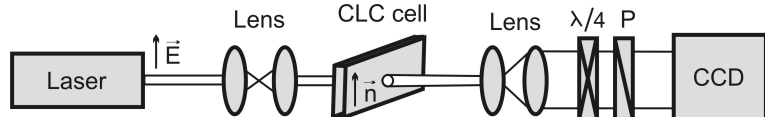


Figure 4: Scheme of the polarimeter. Setup consists of a He-Ne laser ($\lambda = 633$ nm), collimating lenses, CLC cell, beam-expander, Stokes analyzer (quarter-wave plate and polarizer) and charge coupled device (CCD) camera.

After each step of uv irradiation, the ellipticity of light transmitted through the cell

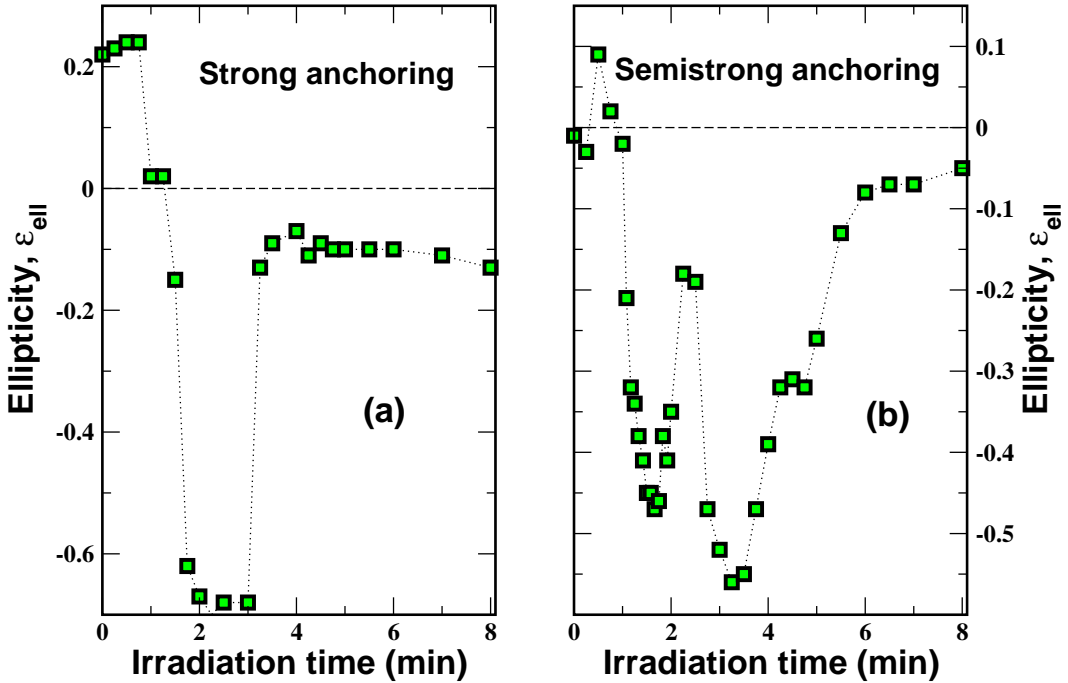


Figure 5: (Color online) (a) Ellipticity ϵ_{ell} of transmitted light measured as a function of uv irradiation time in cells with (a) strong and (b) semistrong anchoring conditions.

was measured using the standard Stokes polarimetry technique which is described in our previous papers [37, 38]. The time interval between irradiation and polarimetry studies was long enough (up to 30 min) to allow for the processes of reorientation to reach the stationary state.

Figure 4 shows the setup scheme used in our experiments. Referring to Fig. 4, the cell is irradiated with a beam generated by a He-Ne laser (the wavelength is 633 nm) and passed through the collimating lenses. After the cell, the beam is expanded and a charge coupled device (CCD) camera collects the output from the Stokes analyzer represented by the combination of the quarter wave plate and the polarizer.

Figure 5 presents the results for the ellipticity measured at different irradiation doses in the symmetric and asymmetric CLC cells. These results were derived using the standard procedure [32–35] which involves performing the intensity measurements at six different combinations of the quarter wave plate and the polarizer needed to obtain the Stokes parameters.

The theoretical results shown in Fig. 6 are computed from the analytical expression for the transmission matrix deduced in Appendix A (see formulas (A52a), (A52c) and (A50a)) using the transfer matrix method in the form formulated in Refs. [37, 39]. In particular, the curve depicted in Fig. 6(a) represents the q -dependence of the ellipticity and can be used to estimate the helix pitch P at different irradiation doses by making comparison between the experimental data and the results of calculations. In the subsequent section we provide details on the procedure used for data processing and discuss the results.

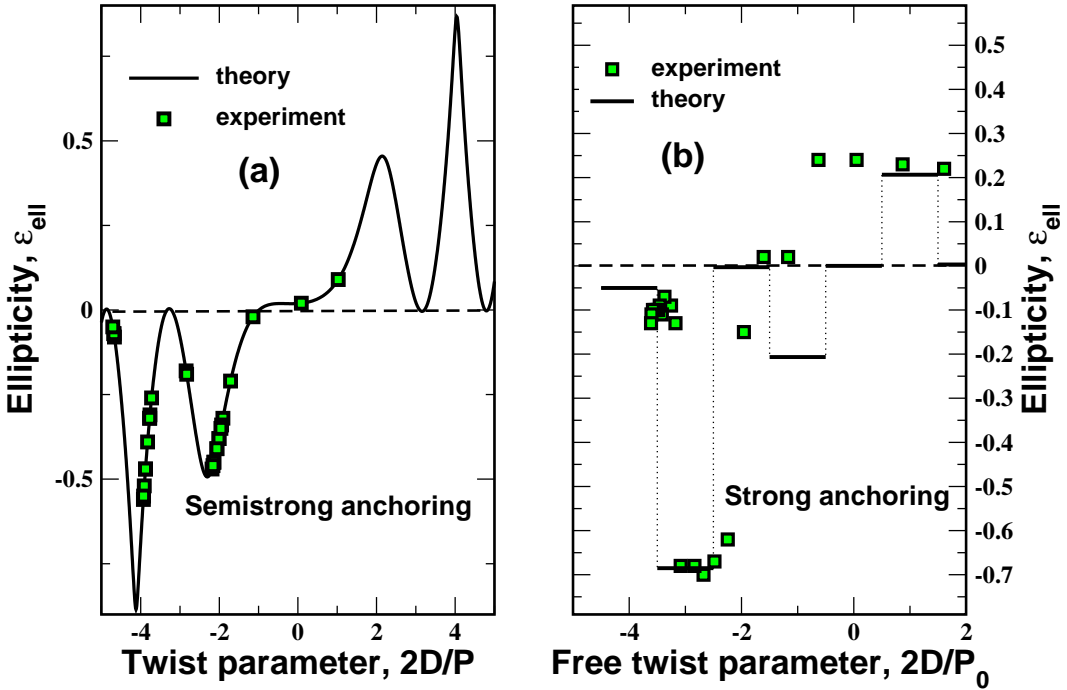


Figure 6: (Color online) (a) Ellipticity ϵ_{ell} computed as a function of the twist parameter, $2D/P$, for light transmitted through a CLC cell of thickness $D = 62 \mu\text{m}$. $\Delta\phi = 3 \text{ deg}$ (see Eq. (A54)) and $n_{\perp} = 1.4674$ ($n_{\parallel} = 1.5191$) is the ordinary (extraordinary) refractive index. Squares indicate the places that are associated with the experimental points by applying the procedure described in Sec. III B. (b) Ellipticity ϵ_{ell} computed for seven equilibrium helical structures ($2D/P \in \{-4, -3, -2, -1, 0, 1, 2\}$) in the symmetric CLC cell for $\Delta\phi = 0 \text{ deg}$. Squares represent the q_0 -dependence of the ellipticity obtained for the experimental data shown in Figs. 5(a) and 2(b).

III. RESULTS

At this stage, our task is to evaluate the pitch of the CLC helical structure formed at different irradiation doses from the results of the previous section. In this section, we detail the procedures used for this purpose and present the results.

A. Strong anchoring: Symmetric cells

When the anchoring is strong at both substrates, the boundary conditions require the CLC director (1) at the substrates to be parallel to the corresponding easy axis (in experiments, the easy axes are defined by the direction of rubbing). Owing to the boundary conditions, the helix wave number q takes values from a discrete set. This set represents the helical structures characterized by the twist parameter $\nu = qD/\pi = 2D/P$ and labeled by the half-turn number k ,

$$\nu \equiv qD/\pi = k, \quad k \in \mathbb{Z}. \quad (3)$$

The equilibrium value of k is the integer that minimizes the distance between k and the free twist parameter $\nu_0 = q_0 D/\pi = 2D/P_0$. The resulting step-like dependence of $2D/P$ on

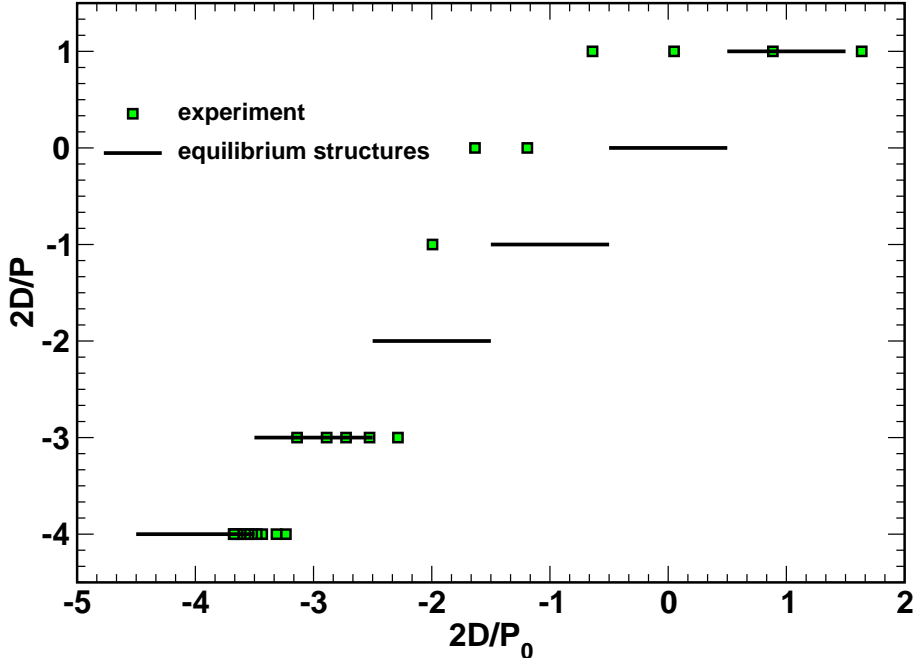


Figure 7: (Color online) Twist parameter $2D/P$ versus free twist parameter $2D/P_0$ measured in the CLC cell with strong anchoring conditions.

$2D/P_0$ for the equilibrium helical structures is depicted in Fig. 7.

According to the stability analysis of Ref. [16], instability caused by slippage of the director in the plane of the spiral cannot occur provided the azimuthal anchoring is strong at both substrates. The structures may, however, lose their stability due to out-of-plane fluctuations. It was shown that, when the energy cost of bending is relatively small, the structure becomes unstable at sufficiently large distance between its wave number q and q_0 [16].

The values of the ellipticity indicated in Fig. 6(b) are calculated for helical structures in the symmetric cell with strong anchoring conditions. From Eq. (3), these structures are characterized by the integer half-turn number $2D/P = k$ which is independent of the free twisting wave number.

The experimental points in Fig. 6(b) represent the dependence of the ellipticity on the free twist parameter $2D/P_0$ that can be obtained from the data shown in Fig. 5(b) with the help of the irradiation time dependence of the free twisting wave number shown in Fig. 2(b). These points can now be related to the half-turn number k , by minimizing both the difference between the theoretical and experimental values of the ellipticity and the change in the half-turn number Δk .

Figure 7 shows the experimental q_0 -dependence of the helix twist parameter $2D/P$ measured in the CLC cells with strong anchoring conditions at both substrates. Referring to Fig. 7, it can be seen that the experimental data indicate the presence of metastable states and jump-like transitions with $\Delta k = 1$ and $\Delta k = 2$.

B. Semistrong anchoring: Asymmetric cells

Asymmetric CLC cells represent the case of mixed boundary conditions in which the strong anchoring limit applies only to the entrance plate, $z = 0$. This case is referred to as semistrong anchoring and we assume that the anchoring potential at the substrate with weak anchoring conditions can be taken in the Rapini-Papouli form [40]:

$$V_s(\phi_s) = \frac{W}{2} \sin^2(\phi_s - \phi_e), \quad (4)$$

where W is the anchoring energy strength, $\phi_s \equiv \phi(D)$ is the director azimuthal angle at the surface and ϕ_e is the azimuthal angle of the easy axis, $\hat{\mathbf{e}} = (\cos \phi_e, \sin \phi_e, 0)$.

For such CLC cells, the relation between the helix wave number and the free twisting wave number can be conveniently written in the following form [16]:

$$\begin{aligned} \nu_0 &= \nu + w/\pi \sin 2(\pi\nu - \phi_e), & w &= \frac{WD}{2K_t}, \\ \nu &= 2D/P, & \nu_0 &= 2D/P_0, \end{aligned} \quad (5)$$

where K_t is the twist elastic constant. The stability condition for the helical configurations characterized by the twisting parameter ν is given by

$$1 + 2w \cos 2(\pi\nu - \phi_e) > 0. \quad (6)$$

Formulas (5) and (6) can be used for processing the experimental data presented in Fig. 5(b). This procedure produces dependence of the twist parameter $2D/P$ on the free twisting parameter $2D/P_0$ based on the data shown in Figs. 5(b) and 2(b) and the ellipticity computed as a function of $2D/P$ [see the theoretical curve in Fig. 6(a)]. It works as follows:

- (a) For each point in Fig. 5(b), the value of the irradiation time is used to compute the corresponding value of the free twisting wave number using the curve depicted in Figs. 2(b).
- (b) For each value of the measured ellipticity in Fig. 5(b) and the associated free twisting parameter, we generally obtain multiple values of the twist parameter representing the points on the theoretical curve in Fig. 6(a) with ellipticity equal to the measured one. The next step describes the selection procedure.
- (c) Given the free twisting parameter and the values of the twist parameter, $2D/P_0 = \nu_0$ and $2D/P = \nu$, we evaluate $1 + 2w \cos 2(\pi\nu - \phi_e)$ and the difference $\Delta = |\nu_0 - \nu - w/\pi \sin 2(\pi\nu - \phi_e)|$. Then we choose the twist parameter that satisfies the stability condition (6) and minimizes Δ . The selected points are indicated by squares in Fig. 6(a).
- (d) The result is that each point in Fig. 5(b) is characterized by the free twisting parameter and the twist parameter. These parameters define the points indicated by squares in Fig. 8.

From Fig. 8, it can be seen that the results for the asymmetric cell are in good agreement with the theoretical predictions of Ref. [16] (Eqs. (5) and (6)). They indicate that the jump-like pitch transitions occur only between the adjacent branches of stable helical structures, unlike in the case of symmetric cell with strong anchoring.

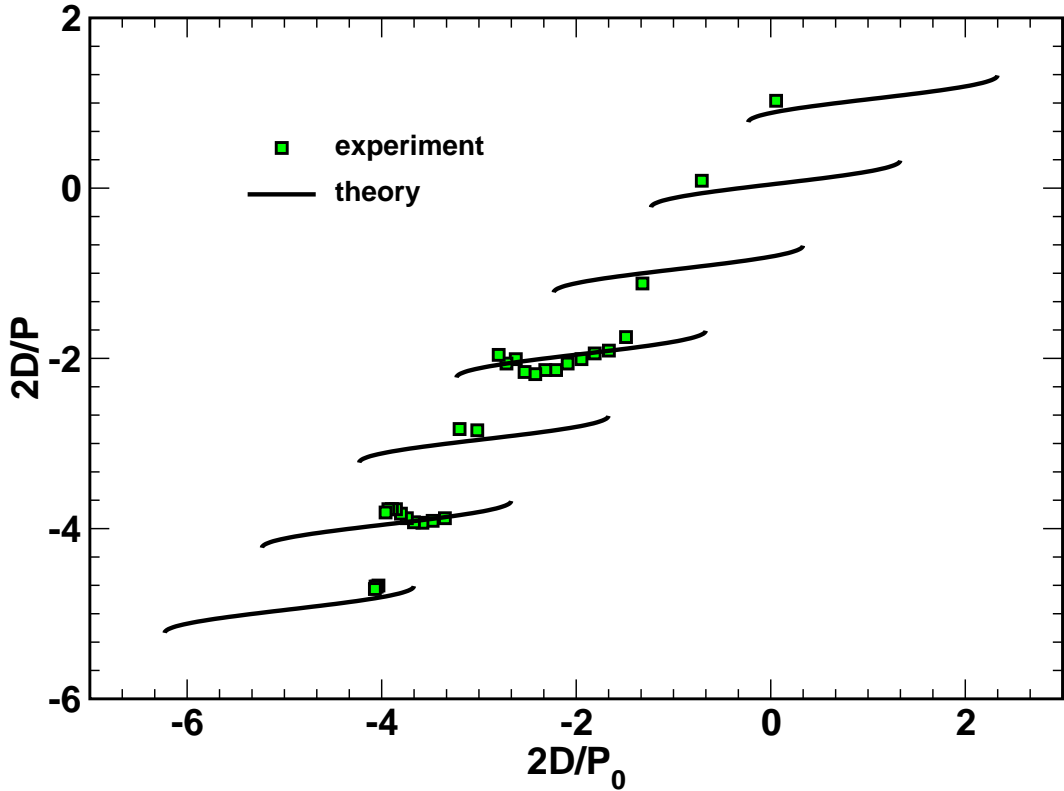


Figure 8: (Color online) Dependence of the twist parameter, $2D/P$, on the free twist parameter, $2D/P_0$, measured in the CLC cell with semistrong anchoring conditions.

Theoretical curve is computed from Eq. (5) at $w = 3.2$ and $\phi_e = 9$ deg. Solid line represents branches of stable twisting states that meet the stability condition (6).

Note that the above procedure relies on the computed curve representing the q -dependence of the ellipticity of light transmitted through the CLC cell. In addition to parameters such as the cell thickness and the refractive indices, this curve depends on the angle between the surface director at the entrance substrate and the polarization vector of the linearly polarized incident light, $\Delta\phi$. It is found that the best fit value of this angle is about 3 deg. This implies that, in the asymmetric cells, the surface director may not be parallel to the rubbing direction. A similar phenomenon was previously reported in Ref. [12]. In our case, however, the angle is relatively small and can be attributed to the misalignment error.

In closing this section, we briefly comment on the estimated value of the anchoring energy parameter, $w \approx 3.2$. For the thickness $D \approx 62 \mu\text{m}$ and the twist elastic constant $K_t \approx 10^{-12} \text{ N}$, the anchoring energy strength can be estimated at about $W = 2wK_t/D \approx 10^{-7} \text{ J/m}^2$. It comes as no surprise that, for the untreated substrate, the estimated anchoring energy is at least two orders of magnitude smaller than typical values for the azimuthal anchoring energy strength [41].

IV. DISCUSSION AND CONCLUSIONS

In the confined geometry of planar cells, the helical structures formed in the cells and their stability are greatly affected by the boundary conditions imposed at the confining surfaces.

The helix pitch characterizing these structures generally differs from its equilibrium value. A more important additional effect is the presence of multiple metastable twisting states in such cells, which appear as a result of interplay between the bulk and the surface contributions to the free energy. Changes of the equilibrium pitch may trigger sharp transitions — the so-called pitch transitions — between different branches of metastable states.

In this paper we have studied the pitch transitions in cells filled with photosensitive chiral nematic liquid crystals. In such materials, the equilibrium pitch can be efficiently controlled by light through photochemically induced transformations of chiral dopants.

In order to determine the concentrations of photoisomers that govern the equilibrium pitch (and the free twisting wave number $q_0 = 2\pi/P_0$) we have used the method of uv absorption spectroscopy combined with modeling the kinetics of the photoreaction. In our experiments, the free twisting wave number is found to be a monotonically decreasing function of irradiation time [see Fig. 2(b)].

The pitch of helical structures formed in the cells after each step of irradiation was estimated from the experimental results of polarimetry measurements giving the ellipticity of light transmitted through the cells at different irradiation doses (see Fig. 5). There are two cases that have been studied experimentally: (a) a symmetric cell with strong anchoring conditions at both substrates; and (b) an asymmetric cell with mixed boundary conditions where weak anchoring conditions are applied at one of the substrates (semistrong anchoring).

From the steplike dependence of the twist parameter $\nu = 2D/P$ on the free twist parameter $\nu_0 = 2D/P_0$ shown in Fig. 7, it can be concluded that the light-induced pitch transitions in the symmetric cell are governed by the boundary conditions and involve metastable twisting states. By contrast, the similar dependence for the asymmetric cell with semistrong anchoring (see Fig. 8) shows successive jumplike transitions that take place between the branches of stable twisting states where the twist parameter ν monotonically increases with ν_0 .

We have found that such behavior agrees very well with the predictions of the theoretical analysis performed in Ref. [16]. According to this analysis, the helical structure responds to variations of the free wave number q_0 (and thus the free twist parameter ν_0) by changing its twist parameter ν . This change may render the initially equilibrium structure either metastable or unstable. Under certain conditions, this instability is governed by in-plane director fluctuations. The mechanism dominating transformations of the director field then can be described as director slippage through the energy barriers formed by the surface potentials.

For the case of semistrong anchoring, equations (5) and (6) define branches of stable helical structures. These formulas were used to fit the experimental data and the best fit value of the anchoring energy parameter is estimated at about $w = WD/(2K_t) \approx 3.2$. So, the anchoring energy strength at the untreated substrate is found to be at least two orders of magnitude smaller than typical values of the azimuthal anchoring strength. It turns out that this value is not small enough to suppress the jump-like behavior. From Eq. (6), the latter occurs at $w < 1$.

In conclusion, it should be emphasized that the non-equilibrium dynamics of the light-induced pitch transitions is well beyond the scope of this paper. We have demonstrated that use of photosensitive CLCs with light controlled equilibrium pitch provides a useful tool for investigation of such transitions and we hope that our study will stimulate further progress in this field.

Appendix A: Optics of helical structures at normal incidence: exact solution revisited

In this appendix we briefly outline the transfer matrix approach in the form formulated in Refs. [37, 39, 42] and show how it can be used to describe the optical properties of ideal CLC helical structures. The director field of these structures is given in Eq. (1) and is characterized by the helix wave number $q = 2\pi/P$, where P is the CLC pitch.

1. Transfer matrix method

We deal with a harmonic electromagnetic field characterized by the free-space wave number $k_{\text{vac}} = \omega/c$, where ω is the frequency (the time-dependent factor is $\exp\{-\omega t\}$), and consider the slab geometry. In this geometry, an optically anisotropic layer of thickness D is sandwiched between the bounding surfaces (substrates): $z = 0$ and $z = D$ (the z axis is normal to the substrates) and is characterized by the dielectric tensor ϵ_{ij} and the magnetic permittivity μ . The dielectric tensor can be expressed in terms of the director (1) as follows

$$\epsilon_{ij}(z) = \epsilon_{\perp} \delta_{ij} + \Delta\epsilon n_i(z) n_j(z), \quad \Delta\epsilon = \epsilon_{\parallel} - \epsilon_{\perp}, \quad (\text{A1})$$

where δ_{ij} is the Kronecker symbol and $n_{\perp} = \sqrt{\mu\epsilon_{\perp}}$ ($n_{\parallel} = \sqrt{\mu\epsilon_{\parallel}}$) is the ordinary (extraordinary) refractive index.

Further, we restrict ourselves to the case of stratified media and assume that the electromagnetic fields can be taken in the following factorized form

$$\{\mathbf{E}(\mathbf{r}), \mathbf{H}(\mathbf{r})\} = \{\mathbf{E}(z), \mathbf{H}(z)\} \exp(\mathbf{k}_p \cdot \mathbf{r}), \quad (\text{A2})$$

where the vector

$$\mathbf{k}_p/k_{\text{vac}} = \mathbf{q}_p = q_p(\cos\phi_p, \sin\phi_p, 0) \quad (\text{A3})$$

represents the lateral component of the wave vector. Then we write down the representation for the electric and magnetic fields, \mathbf{E} and \mathbf{H} ,

$$\mathbf{E} = E_z \hat{\mathbf{z}} + \mathbf{E}_P, \quad \mathbf{H} = H_z \hat{\mathbf{z}} + \hat{\mathbf{z}} \times \mathbf{H}_P, \quad (\text{A4})$$

where the components directed along the normal to the bounding surface (the z axis) are separated from the tangential (lateral) ones. In this representation, the vectors $\mathbf{E}_P = E_x \hat{\mathbf{x}} + E_y \hat{\mathbf{y}} \equiv \begin{pmatrix} E_x \\ E_y \end{pmatrix}$ and $\mathbf{H}_P = \mathbf{H} \times \hat{\mathbf{z}} \equiv \begin{pmatrix} H_y \\ -H_x \end{pmatrix}$ are parallel to the substrates and give the lateral components of the electromagnetic field.

Substituting the relations (A4) into the Maxwell equations and eliminating the z components of the electric and magnetic fields gives equations for the tangential components of the electromagnetic field that can be written in the following 4×4 matrix form [37]:

$$-i\partial_{\tau} \mathbf{F} = \mathbf{M} \mathbf{F} \equiv \begin{pmatrix} \mathbf{M}_{11} & \mathbf{M}_{12} \\ \mathbf{M}_{21} & \mathbf{M}_{22} \end{pmatrix} \begin{pmatrix} \mathbf{E}_P \\ \mathbf{H}_P \end{pmatrix}, \quad \tau \equiv k_{\text{vac}} z. \quad (\text{A5})$$

For the dielectric tensor (A1) with the plane of incidence parallel to the x - z plane, from the general expressions derived in Refs. [37, 39], the 2×2 matrices \mathbf{M}_{ij} characterizing the block structure of the matrix \mathbf{M} are given by

$$\mathbf{M}_{12} = \mu \mathbf{I}_2 - \frac{q_p^2}{2\epsilon_{\perp}} (\mathbf{I}_2 + \boldsymbol{\sigma}_3), \quad \mathbf{M}_{ii} = \mathbf{0}, \quad (\text{A6})$$

$$\mathbf{M}_{21} = -\frac{q_p^2}{2\mu} (\mathbf{I}_2 - \boldsymbol{\sigma}_3) + \epsilon_c \left\{ \mathbf{I}_2 + u_a [\cos(2\phi) \boldsymbol{\sigma}_3 + \sin(2\phi) \boldsymbol{\sigma}_1] \right\}, \quad (\text{A7})$$

$$\epsilon_c = (\epsilon_{\parallel} + \epsilon_{\perp})/2, \quad u_a = \frac{\epsilon_{\parallel} - \epsilon_{\perp}}{\epsilon_{\parallel} + \epsilon_{\perp}}, \quad (\text{A8})$$

$$\phi = \tilde{q}\tau + \phi_0, \quad \tilde{q} = q/k_{\text{vac}} = \lambda/P, \quad (\text{A9})$$

where \mathbf{I}_n is the $n \times n$ identity matrix and $\{\boldsymbol{\sigma}_1, \boldsymbol{\sigma}_2, \boldsymbol{\sigma}_3\}$ are the Pauli matrices given by

$$\boldsymbol{\sigma}_1 = \begin{pmatrix} 0 & 1 \\ 1 & 0 \end{pmatrix}, \quad \boldsymbol{\sigma}_2 = \begin{pmatrix} 0 & -i \\ i & 0 \end{pmatrix}, \quad \boldsymbol{\sigma}_3 = \begin{pmatrix} 1 & 0 \\ 0 & -1 \end{pmatrix}. \quad (\text{A10})$$

General solution of the system (A5)

$$\mathbf{F}(\tau) = \mathbf{U}(\tau, \tau_0) \mathbf{F}(\tau_0) \quad (\text{A11})$$

can be conveniently expressed in terms of the *evolution operator* defined as the matrix solution of the initial value problem

$$-i\partial_{\tau} \mathbf{U}(\tau, \tau_0) = \mathbf{M}(\tau) \mathbf{U}(\tau, \tau_0), \quad (\text{A12a})$$

$$\mathbf{U}(\tau_0, \tau_0) = \mathbf{I}_4, \quad (\text{A12b})$$

In the ambient medium with $\epsilon_{ij} = \epsilon_m \delta_{ij}$ and $\mu = \mu_m$, the general solution (A11) can be expressed in terms of plane waves propagating along the wave vectors with the tangential component (A3). For such waves, the result is given by [42]

$$\mathbf{F}_m(\tau) = \mathbf{V}_m(\mathbf{q}_p) \begin{pmatrix} \exp\{i\mathbf{Q}_m \tau\} & \mathbf{0} \\ \mathbf{0} & \exp\{-i\mathbf{Q}_m \tau\} \end{pmatrix} \begin{pmatrix} \mathbf{E}_+ \\ \mathbf{E}_- \end{pmatrix}, \quad (\text{A13})$$

$$\mathbf{Q}_m = q_m \mathbf{I}_2, \quad q_m = \sqrt{n_m^2 - q_p^2}, \quad (\text{A14})$$

where $\mathbf{V}_m(\mathbf{q}_p)$ is the eigenvector matrix for the ambient medium given by

$$\mathbf{V}_m(\mathbf{q}_p) = \mathbf{T}_{\text{rot}}(\phi_p) \mathbf{V}_m = \begin{pmatrix} \mathbf{Rt}(\phi_p) & \mathbf{0} \\ \mathbf{0} & \mathbf{Rt}(\phi_p) \end{pmatrix} \begin{pmatrix} \mathbf{E}_m & -\boldsymbol{\sigma}_3 \mathbf{E}_m \\ \mathbf{H}_m & \boldsymbol{\sigma}_3 \mathbf{H}_m \end{pmatrix}, \quad (\text{A15})$$

$$\mathbf{E}_m = \begin{pmatrix} q_m/n_m & 0 \\ 0 & 1 \end{pmatrix}, \quad \mu_m \mathbf{H}_m = \begin{pmatrix} n_m & 0 \\ 0 & q_m \end{pmatrix}, \quad (\text{A16})$$

$$\mathbf{Rt}(\phi) = \begin{pmatrix} \cos \phi & -\sin \phi \\ \sin \phi & \cos \phi \end{pmatrix}, \quad (\text{A17})$$

From Eq. (A13), the vector amplitudes \mathbf{E}_+ and \mathbf{E}_- correspond to the forward and backward eigenwaves with $\mathbf{k}_+ = k_{\text{vac}}(q_m \hat{\mathbf{z}} + \mathbf{q}_p)$ and $\mathbf{k}_- = k_{\text{vac}}(-q_m \hat{\mathbf{z}} + \mathbf{q}_p)$, respectively. In the half space $z \leq 0$ before the entrance face of the layer $z = 0$, these eigenwaves describe the *incident and reflected waves*

$$\mathbf{E}_+|_{z \leq 0} = \mathbf{E}_{\text{inc}}, \quad \mathbf{E}_-|_{z \leq 0} = \mathbf{E}_{\text{refl}}, \quad (\text{A18})$$

whereas, in the half space $z \geq D$ after the exit face of the layer, these waves are given by

$$\mathbf{E}_+|_{z \geq D} = \mathbf{E}_{\text{trm}}, \quad \mathbf{E}_-|_{z \geq D} = 0, \quad (\text{A19})$$

where \mathbf{E}_{trm} is the vector amplitude of the *transmitted wave*. The standard linear input-output relations

$$\mathbf{E}_{\text{trm}} = \mathbf{T} \mathbf{E}_{\text{inc}}, \quad \mathbf{E}_{\text{refl}} = \mathbf{R} \mathbf{E}_{\text{inc}} \quad (\text{A20})$$

link the vector amplitudes of transmitted and reflected waves \mathbf{E}_{trm} and \mathbf{E}_{refl} with the amplitude of the incident wave \mathbf{E}_{inc} through the transmission and reflection matrices \mathbf{T} and \mathbf{R} .

It is our task now to relate these matrices and the evolution operator given by Eq. (A12). To this end, we use the boundary conditions requiring the tangential components of the electric and magnetic fields to be continuous at the boundary surfaces: $\mathbf{F}(0) = \mathbf{F}_m(0 - 0)$ and $\mathbf{F}(h) = \mathbf{F}_m(h + 0)$, and apply the relation (A12) to the anisotropic layer of the thickness D to yield the following result

$$\mathbf{F}_m(h + 0) = \mathbf{U}(h, 0) \mathbf{F}_m(0 - 0), \quad h = k_{\text{vac}} D. \quad (\text{A21})$$

On substituting Eqs. (A13) into Eq. (A21) we have

$$\begin{pmatrix} \mathbf{E}_{\text{inc}} \\ \mathbf{E}_{\text{refl}} \end{pmatrix} = \mathbf{W} \begin{pmatrix} \mathbf{E}_{\text{trm}} \\ \mathbf{0} \end{pmatrix} \quad (\text{A22})$$

where the matrix \mathbf{W} linking the electric field vector amplitudes of the waves in the half spaces $z < 0$ and $z > D$ bounded by the faces of the layer will be referred to as the *transfer (linking) matrix*. The expression for the transfer matrix is as follows

$$\mathbf{W} = \mathbf{V}_m^{-1} \mathbf{U}_R^{-1}(h) \mathbf{V}_m = \begin{pmatrix} \mathbf{W}_{11} & \mathbf{W}_{12} \\ \mathbf{W}_{21} & \mathbf{W}_{22} \end{pmatrix} \quad (\text{A23})$$

where $\mathbf{U}_R(\tau) = \mathbf{T}_{\text{rot}}(-\phi_p) \mathbf{U}(\tau, 0) \mathbf{T}_{\text{rot}}(\phi_p)$ is the rotated operator of evolution. This operator is the solution of the initial value problem (A12) with $\mathbf{M}(\tau)$ replaced by $\mathbf{M}_R(\tau) = \mathbf{T}_{\text{rot}}(-\phi_p) \mathbf{M}(\tau) \mathbf{T}_{\text{rot}}(\phi_p)$.

From Eqs. (A20), and (A22), the transmission and reflection matrices can be expressed in terms of the transfer matrix as follows

$$\mathbf{T} = \mathbf{W}_{11}^{-1}, \quad \mathbf{R} = \mathbf{W}_{21} \mathbf{T}. \quad (\text{A24})$$

In what follows we assume that, as is illustrated in Fig. 3, the light impinges normally onto the CLC cell with $q_p = 0$ and $\phi_p = 0$. So, all the waves are propagating along the helical axis and we deal with the most studied limiting case of normal incidence, which has a long history dating back more than half a century to the original paper by De Vries [43].

2. Operator of evolution: rotating wave ansatz

By contrast to the case of oblique incidence, it can be shown that the initial value problem for the evolution operator (A12) is exactly solvable at $q_p = 0$. To this end, we begin with the vector amplitudes written in the circular basis

$$\mathbf{E}_\alpha = E_x^{(\alpha)} \hat{\mathbf{x}} + E_y^{(\alpha)} \hat{\mathbf{y}} = E_+^{(\alpha)} \hat{\mathbf{e}}_+ + E_-^{(\alpha)} \hat{\mathbf{e}}_-, \quad (\text{A25})$$

where $\hat{\mathbf{e}}_\pm = (\hat{\mathbf{x}} \pm i \hat{\mathbf{y}})/\sqrt{2}$ and $E_\pm^{(\alpha)} = (E_x^{(\alpha)} \mp i E_y^{(\alpha)})/\sqrt{2}$, so that the transfer and reflection matrices

$$\mathbf{T}_C = \mathbf{C} \mathbf{T} \mathbf{C}^\dagger, \quad \mathbf{R}_C = \mathbf{C} \mathbf{R} \mathbf{C}^\dagger, \quad (\text{A26})$$

where $\mathbf{C} = \frac{1}{\sqrt{2}} \begin{pmatrix} 1 & -i \\ 1 & i \end{pmatrix}$, relate the circular components of the incident, transmitted and reflected waves. When the basis changes the system (A5) transforms and, in the circular basis, takes the following form

$$-i\partial_\tau \mathbf{F}_C = \mathbf{M}_C \mathbf{F}_C, \quad \mathbf{M}_C = \tilde{\mathbf{C}} \mathbf{M} \tilde{\mathbf{C}}^\dagger, \quad (\text{A27})$$

$$\mathbf{F}_C = \tilde{\mathbf{C}} \mathbf{F}, \quad \tilde{\mathbf{C}} = \begin{pmatrix} \mathbf{C} & \mathbf{0} \\ \mathbf{0} & \mathbf{C} \end{pmatrix}. \quad (\text{A28})$$

The next step is the rotating wave ansatz that uses the basis vectors rotating in helical fashion similarly to the director field. For the electric field, it can be written in the following form:

$$\mathbf{E} = E_x^{(\text{rw})} \hat{\mathbf{n}} + E_y^{(\text{rw})} \hat{\mathbf{m}} = E_+^{(\text{rw})} \hat{\mathbf{e}}_+^{(\text{rw})} + E_-^{(\text{rw})} \hat{\mathbf{e}}_-^{(\text{rw})} \quad (\text{A29})$$

where $\hat{\mathbf{e}}_\pm^{(\text{rw})} = \exp\{\mp i\phi\} \hat{\mathbf{e}}_\pm = (\hat{\mathbf{n}} \pm i \hat{\mathbf{m}})/\sqrt{2}$ and the unit vector $\hat{\mathbf{m}} = \hat{\mathbf{z}} \times \hat{\mathbf{n}} = \partial_\phi \hat{\mathbf{n}}$ is perpendicular to the director $\hat{\mathbf{n}}$ defined in Eq. (1). More generally, this ansatz is defined as follows

$$\mathbf{F}_{\text{RW}} = \mathbf{R}_+(\phi) \mathbf{F}_C, \quad (\text{A30})$$

$$\mathbf{R}_\pm(\phi) = \begin{pmatrix} \exp\{i\phi \boldsymbol{\sigma}_3\} & \mathbf{0} \\ \mathbf{0} & \exp\{\pm i\phi \boldsymbol{\sigma}_3\} \end{pmatrix} \quad (\text{A31})$$

so that Eq. (A27) is transformed into the system

$$\begin{aligned} -i\partial_\tau \mathbf{F}_{\text{RW}} &= \mathbf{M}_{\text{RW}} \mathbf{F}_{\text{RW}} = \\ &= \begin{pmatrix} \tilde{q} \boldsymbol{\sigma}_3 & \mu \mathbf{I}_2 \\ \epsilon_c \{ \mathbf{I}_2 + u_a \boldsymbol{\sigma}_1 \} & \tilde{q} \boldsymbol{\sigma}_3 \end{pmatrix} \begin{pmatrix} \mathbf{E}_{\text{RW}} \\ \mathbf{H}_{\text{RW}} \end{pmatrix}, \end{aligned} \quad (\text{A32})$$

where the matrix \mathbf{M}_{RW} is independent of τ .

The evolution operator of the system (A32) then can be readily expressed in terms of eigenvalues and eigenvectors of the matrix \mathbf{M}_{RW} . The result is given by

$$\begin{aligned} \mathbf{U}_{\text{RW}}(\tau) &= \exp\{i\mathbf{M}_{\text{RW}} \tau\} = \\ &= \mathbf{V} \begin{pmatrix} \mathbf{U}_+(n_c \tau) & \mathbf{0} \\ \mathbf{0} & \mathbf{U}_-(n_c \tau) \end{pmatrix} \mathbf{V}^{-1}, \quad n_c^2 = \mu \epsilon_c, \end{aligned} \quad (\text{A33})$$

$$\mathbf{U}_\pm(\tau) = \exp\{\pm i\boldsymbol{\Lambda} \tau\}, \quad \boldsymbol{\Lambda} = \begin{pmatrix} \kappa_1 & 0 \\ 0 & \kappa_2 \end{pmatrix}, \quad (\text{A34})$$

where

$$\kappa_{1,2} = \left[1 + q_c^2 \pm \sqrt{4q_c^2 + u_a^2} \right]^{1/2}, \quad q_c = \tilde{q}/n_c, \quad (\text{A35})$$

$$\mathbf{V} = \begin{pmatrix} \mathbf{E} & -\boldsymbol{\sigma}_1 \mathbf{E} \\ \mathbf{H} & \boldsymbol{\sigma}_1 \mathbf{H} \end{pmatrix}, \quad \mathbf{E} = (\mathbf{E}_1 \mathbf{E}_2), \quad \mathbf{H} = (\mathbf{H}_1 \mathbf{H}_2) \quad (\text{A36})$$

$$\mathbf{E}_i = \begin{pmatrix} u_a \\ (\kappa_i - q_c)^2 - 1 \end{pmatrix}, \quad \mathbf{H}_i = \frac{n_c}{\mu} [\kappa_i \mathbf{I}_2 - q_c \boldsymbol{\sigma}_3] \mathbf{E}_i. \quad (\text{A37})$$

Note that the eigenvector matrix (A36) satisfies orthogonality conditions of the form [37]

$$\mathbf{V}^{-1} = \mathbf{N}^{-1} \mathbf{V}^T \mathbf{G}, \quad (\text{A38})$$

$$\mathbf{N} = \text{diag}(\mathbf{N}_+, -\mathbf{N}_+), \quad \mathbf{N}_+ = \text{diag}(N_1, N_2), \quad (\text{A39})$$

$$N_i = \frac{2n_c}{\mu} \{ (\kappa_i - q_c) u_a^2 + (\kappa_i + q_c) [(\kappa_i - q_c)^2 - 1]^2 \}, \quad (\text{A40})$$

and one of the eigenvalues (A35), κ_2 , is imaginary in the optical stop band (photonic bandgap):

$$\kappa_2 = i|\kappa_2|, \quad q_- \equiv \sqrt{1 - |u_a|} \leq |q_c| \leq q_+ \equiv \sqrt{1 + |u_a|}, \quad (\text{A41})$$

where the corresponding eigenmode becomes evanescent and selective reflection takes place. In the photonic bandgap, additional analysis is required so as to deal with the problem of numerical instability caused by the presence of exponentially large terms proportional to $\exp(|\kappa_2| h_c)$. This analysis is given in Sec. A 4.

We can now write down the resulting expression for the evolution operator of the system (A28):

$$\mathbf{U}_C(\tau) = \mathbf{R}_+(-\phi) \mathbf{U}_{\text{RW}}(\tau) \mathbf{R}_+(\phi_0). \quad (\text{A42})$$

3. Transmission and reflection matrices

In the case of normal incidence with $q_p = 0$ and $\phi_p = 0$, the eigenvector matrix for the ambient medium in the circular basis and the corresponding orthogonality relation are given by

$$\mathbf{V}_m = \begin{pmatrix} \mathbf{I}_2 & -\boldsymbol{\sigma}_1 \\ \frac{n_m}{\mu_m} \mathbf{I}_2 & \frac{n_m}{\mu_m} \boldsymbol{\sigma}_1 \end{pmatrix}, \quad \mathbf{V}_m^{-1} = \mathbf{N}_m^{-1} \mathbf{V}_m^T \mathbf{G}, \quad (\text{A43})$$

$$\mathbf{N}_m = N_m \mathbf{G}_3, \quad \mathbf{G}_3 = \text{diag}(\mathbf{I}_2, -\mathbf{I}_2), \quad N_m = 2n_m. \quad (\text{A44})$$

For the evolution operator (A42), these formulas and the relation

$$\mathbf{R}_+(\phi) \mathbf{V}_m = \mathbf{V}_m \mathbf{R}_-(\phi) \quad (\text{A45})$$

can now be used to deduce the transfer matrix (A23) in the following form:

$$\mathbf{W} = \mathbf{R}_-(-\phi_0) \mathbf{W}_{\text{RW}} \mathbf{R}_-(\phi_1), \quad \phi_1 = \phi_0 + \pi \nu \quad (\text{A46})$$

$$\mathbf{W}_{\text{RW}} = \mathbf{V}_2 \begin{pmatrix} \mathbf{U}_-(h_c) & \mathbf{0} \\ \mathbf{0} & \mathbf{U}_+(h_c) \end{pmatrix} \mathbf{V}_2^{-1}, \quad h_c = n_c h, \quad (\text{A47})$$

$$N_m \mathbf{V}_2 = \begin{pmatrix} \mathbf{A}_+ & \mathbf{A}_- \\ \mathbf{A}_- & \mathbf{A}_+ \end{pmatrix}, \quad \tilde{\mathbf{N}}_+ \mathbf{V}_2^{-1} = \begin{pmatrix} \mathbf{A}_+^T & -\mathbf{A}_-^T \\ -\mathbf{A}_-^T & \mathbf{A}_+^T \end{pmatrix}, \quad (\text{A48})$$

where $\nu = 2D/P = q_c h_c / \pi$ is the CLC half-turn number parameter; $\mathbf{V}_2 \equiv \mathbf{V}_m^{-1} \mathbf{V}$ and $\tilde{\mathbf{N}}_+ \equiv \text{diag}(\mathbf{N}_+, \mathbf{N}_+)$. The matrices \mathbf{A}_+ and \mathbf{A}_- are given by

$$\begin{aligned}\mathbf{A}_+ &= \frac{n_m}{\mu_m} \mathbf{E} + \mathbf{H} = (\mathbf{a}_1^{(+)} \mathbf{a}_2^{(+)}) , \\ \mathbf{A}_- &= \boldsymbol{\sigma}_1 \left\{ -\frac{n_m}{\mu_m} \mathbf{E} + \mathbf{H} \right\} = (\mathbf{a}_1^{(-)} \mathbf{a}_2^{(-)})\end{aligned}\quad (\text{A49})$$

and define the block 2×2 matrices, $\mathbf{W}_{ij}^{(\text{rw})}$, of the transfer matrix (A47) as follows

$$N_m \mathbf{W}_{11}^{(\text{rw})} = \mathbf{A}_+ \mathbf{W}_- \mathbf{A}_+^T - \mathbf{A}_- \mathbf{W}_+ \mathbf{A}_-^T, \quad (\text{A50a})$$

$$\begin{aligned}N_m \mathbf{W}_{21}^{(\text{rw})} &= \mathbf{A}_- \mathbf{W}_- \mathbf{A}_+^T - \mathbf{A}_+ \mathbf{W}_+ \mathbf{A}_-^T = \\ &- N_m [\mathbf{W}_{12}^{(\text{rw})}]^T,\end{aligned}\quad (\text{A50b})$$

$$N_m \mathbf{W}_{22}^{(\text{rw})} = \mathbf{A}_+ \mathbf{W}_+ \mathbf{A}_+^T - \mathbf{A}_- \mathbf{W}_- \mathbf{A}_-^T, \quad (\text{A50c})$$

where

$$\begin{aligned}\mathbf{W}_\mp &= \mathbf{U}_\mp(h_c) \mathbf{N}_+^{-1} = \begin{pmatrix} \gamma_{\pm 1}/N_1 & 0 \\ 0 & \gamma_{\pm 2}/N_2 \end{pmatrix}, \\ \gamma_{\pm i} &= \exp(\mp i \kappa_i h_c).\end{aligned}\quad (\text{A51})$$

Finally, for the transmission and reflection matrices (A24) in the circular basis, we have the relations

$$\mathbf{T}_C = \exp[-i\phi_1 \boldsymbol{\sigma}_3] \mathbf{T}_{RW} \exp[i\phi_0 \boldsymbol{\sigma}_3], \quad (\text{A52a})$$

$$\mathbf{R}_C = \exp[i\phi_0 \boldsymbol{\sigma}_3] \mathbf{R}_{RW} \exp[i\phi_0 \boldsymbol{\sigma}_3], \quad (\text{A52b})$$

$$\mathbf{T}_{RW} = [\mathbf{W}_{11}^{(\text{rw})}]^{-1}, \quad \mathbf{R}_{RW} = \mathbf{W}_{21}^{(\text{rw})} \mathbf{T}_{RW}, \quad (\text{A52c})$$

where the block 2×2 matrices are given in Eqs. (A50a) and (A50b).

Note that the theoretical curves presented in Fig. 6 are computed for the ellipticity

$$\epsilon_{\text{ell}} = \frac{|E_+^{(\text{trm})}| - |E_-^{(\text{trm})}|}{|E_+^{(\text{trm})}| + |E_-^{(\text{trm})}|} \quad (\text{A53})$$

of the transmitted wave

$$\begin{aligned}\exp[i\phi_1 \boldsymbol{\sigma}_3] \begin{pmatrix} E_+^{(\text{trm})} \\ E_-^{(\text{trm})} \end{pmatrix} &= \\ \mathbf{T}_{RW} \exp[i\Delta\phi \boldsymbol{\sigma}_3] \begin{pmatrix} 1 \\ 1 \end{pmatrix} E_0^{(\text{inc})}, \quad \Delta\phi &= \phi_0 - \phi_p^{(\text{inc})},\end{aligned}\quad (\text{A54})$$

where $E_0^{(\text{inc})}$ and $\phi_p^{(\text{inc})}$ are the amplitude and polarization azimuth of the linearly polarized incident wave, respectively.

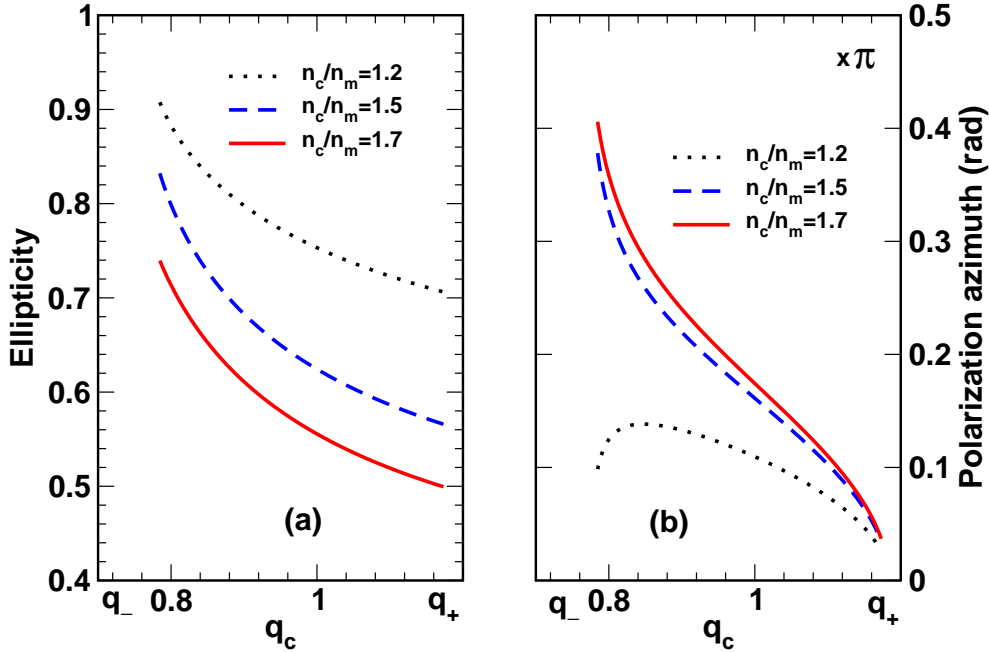


Figure 9: (Color online) Ellipticity and polarization azimuthal angle of light transmitted through a thick CLC layer as a function of the parameter q_c at different values of the optical contrast n_c/n_m .

4. Analytical treatment in photonic band gap

In the photonic band gap (see Eq. (A41)), the eigenvalue parameter

$$\gamma \equiv \gamma_{+2} = \exp(|\kappa_2| h_c) \quad (\text{A55})$$

is large. Since formulas (A52c) for the transmission and reflection matrices contain both large and small terms proportional to γ and γ^{-1} , they cannot be directly applied for numerical analysis.

In this section we derive the analytical results applicable in the optical stop band. For this purpose, we shall use the dyadic representation for the transfer matrix (A47)

$$\begin{aligned} \mathbf{W}_{\text{RW}} = & \sum_{\alpha=\{\pm 1, \pm 2\}} \gamma_{\alpha} \mathbf{v}_{\alpha} \otimes \mathbf{u}_{\alpha} = \\ & \gamma \mathbf{v} \otimes \mathbf{u} + \Gamma, \quad \Gamma = \sum_{\alpha' \neq \pm 2} \gamma_{\alpha'} \mathbf{v}_{\alpha'} \otimes \mathbf{u}_{\alpha'}, \end{aligned} \quad (\text{A56})$$

where the vectors

$$\mathbf{v}_{\pm i} = \begin{pmatrix} \mathbf{P}_1[\mathbf{v}_{\pm i}] \\ \mathbf{P}_2[\mathbf{v}_{\pm i}] \end{pmatrix} = N_m^{-1} \begin{pmatrix} \mathbf{a}_i^{(\pm)} \\ \mathbf{a}_i^{(\mp)} \end{pmatrix}, \quad \mathbf{u}_{\pm i} = \begin{pmatrix} \mathbf{P}_1[\mathbf{u}_{\pm i}] \\ \mathbf{P}_2[\mathbf{u}_{\pm i}] \end{pmatrix} = \pm N_i^{-1} \begin{pmatrix} \mathbf{a}_i^{(\pm)} \\ -\mathbf{a}_i^{(\mp)} \end{pmatrix} \quad (\text{A57})$$

are expressed in terms of the vector-columns, $\mathbf{a}_i^{(\pm)}$, given in Eq. (A49) and form a biorthogonal set: $(\mathbf{v}_{\alpha} \cdot \mathbf{u}_{\alpha'}) = \delta_{\alpha \alpha'}$. The latter follows because columns of the matrix \mathbf{V}_2 and rows of the inverse matrix \mathbf{V}_2^{-1} (see Eq. (A48)) give the components of \mathbf{v}_{α} and \mathbf{u}_{α} , respectively.

From Eqs. (A56) and (A57), the block 2×2 matrices can be similarly rewritten in the dyadic form:

$$N_m N_2 \mathbf{W}_{ij}^{(\text{rw})} = N_m N_2 \sum_{\alpha} \gamma_{\alpha} \mathbf{P}_i[\mathbf{v}_{\alpha}] \otimes \mathbf{P}_j[\mathbf{u}_{\alpha}] = \gamma \mathbf{A}_{ij} + \mathbf{\Gamma}_{ij}. \quad (\text{A58})$$

The transmission matrix (A52c) is expressed in terms of $\mathbf{W}_{11}^{(\text{rw})}$ which is defined by the matrices

$$\mathbf{A}_{11} = \mathbf{a}_2^{(+)} \otimes \mathbf{a}_2^{(+)}, \quad (\text{A59})$$

$$\mathbf{\Gamma}_{11} = N_2/N_1 \sum_{s=\pm} s \gamma_{s1} \mathbf{a}_1^{(s)} \otimes \mathbf{a}_1^{(s)} + \gamma^{-1} \mathbf{a}_2^{(-)} \otimes \mathbf{a}_2^{(-)} \quad (\text{A60})$$

that enter the right hand side of Eq. (A58).

Our task is to derive analytical expression for the transmission matrix that does not contain large terms proportional to γ . To this end, we shall use the relations for 2×2 matrices

$$\mathbf{A}^{-1} = [\det \mathbf{A}]^{-1} \mathbf{A}^{\perp}, \quad \mathbf{A}^{\perp} = \boldsymbol{\sigma}_2 \cdot \mathbf{A}^T \cdot \boldsymbol{\sigma}_2, \quad (\text{A61})$$

$$|\gamma \mathbf{A}_{11} + \mathbf{\Gamma}_{11}| = \gamma [|\mathbf{A}_{11} + \mathbf{\Gamma}_{11}| - (1 - \gamma^{-1}) |\mathbf{\Gamma}_{11}|], \quad (\text{A62})$$

where $|\mathbf{A}| \equiv \det(\mathbf{A})$ is the determinant of a matrix \mathbf{A} and $\mathbf{A}^{\perp} \equiv \text{adj}(\mathbf{A})$ is the adjugate of a 2×2 matrix \mathbf{A} . It is not difficult to see that, for two dimensional vectors, the adjugate of a dyadic can be written in the following form

$$(\mathbf{x} \otimes \mathbf{y})^{\perp} = \mathbf{y}^{\perp} \otimes \mathbf{x}^{\perp}, \quad (\text{A63})$$

where $\mathbf{x}^{\perp} = -i\boldsymbol{\sigma}_2 \cdot \mathbf{x}$ and $(\mathbf{x}^{\perp} \cdot \mathbf{x}) = 0$.

The transmission matrix (A52c) can now be cast into the form suitable for using in the photonic band gap as follows

$$\mathbf{T}_{\text{RW}} = \frac{N_m N_2}{|\mathbf{A}_{11} + \mathbf{\Gamma}_{11}| - (1 - \gamma^{-1}) |\mathbf{\Gamma}_{11}|} \{ \mathbf{A}_{11}^{\perp} + \gamma^{-1} \mathbf{\Gamma}_{11}^{\perp} \}, \quad (\text{A64a})$$

$$\mathbf{A}_{11}^{\perp} = \mathbf{b}_2^{(+)} \otimes \mathbf{b}_2^{(+)}, \quad (\text{A64b})$$

$$\mathbf{\Gamma}_{11}^{\perp} = N_2/N_1 \sum_{s=\pm} s \gamma_{s1} \mathbf{b}_1^{(s)} \otimes \mathbf{b}_1^{(s)} + \gamma^{-1} \mathbf{b}_2^{(-)} \otimes \mathbf{b}_2^{(-)}, \quad (\text{A64c})$$

$$\mathbf{b}_i^{(s)} = -i\boldsymbol{\sigma}_2 \cdot \mathbf{a}_i^{(s)} = \begin{pmatrix} 0 & -1 \\ 1 & 0 \end{pmatrix} \mathbf{a}_i^{(s)}. \quad (\text{A64d})$$

From Eq. (A64a), it is clear that in the limit of thick cells where $\gamma \rightarrow 0$ the transmission matrix approaches the singular dyadic

$$\mathbf{T}_{\text{RW}} \propto \mathbf{b}_2^{(+)} \otimes \mathbf{b}_2^{(+)}, \quad \gamma^{-1} \rightarrow 0 \quad (\text{A65})$$

defined by the vector $\mathbf{b}_2^{(+)}$. The polarization characteristics of this vector are plotted in Fig. 9 as a function of q_c at different values of the contrast ratio n_c/n_m . For any polarization state of the incident light with $\mathbf{E}_{\text{inc}} \nparallel \exp[-i\phi_0 \boldsymbol{\sigma}_3] \mathbf{a}_2^{(+)}$, the parameters depicted in Fig. 9 determine the ellipticity and the polarization azimuth of the transmitted wave when the

CLC cell is sufficiently thick. Since $(\mathbf{a}_2^{(+)} \cdot \mathbf{b}_2^{(+)}) = 0$, transmission of the incident wave with $\mathbf{E}_{\text{inc}} \parallel \exp[-i\phi_0 \boldsymbol{\sigma}_3] \mathbf{a}_2^{(+)}$ has been completely suppressed in the thick cell limit $\gamma \rightarrow 0$.

Equation (A52c) gives the reflection matrix expressed in terms of the transmission matrix (A64a) and $\mathbf{W}_{21}^{(\text{rw})}$. The latter is defined in Eq. (A58) with the matrices given by

$$\mathbf{A}_{21} = \mathbf{a}_2^{(-)} \otimes \mathbf{a}_2^{(+)}, \quad (\text{A66})$$

$$\mathbf{\Gamma}_{21} = -N_2/N_1 \sum_{s=\pm} s \gamma_{s1} \mathbf{a}_1^{(-s)} \otimes \mathbf{a}_1^{(s)} + \gamma^{-1} \mathbf{a}_2^{(+)} \otimes \mathbf{a}_2^{(-)}. \quad (\text{A67})$$

Similar to the transmission matrix, the reflection matrix can now be written in the following dyadic form:

$$\mathbf{R}_{\text{RW}} = \frac{\mathbf{\Gamma}_{21} \cdot \mathbf{A}_{11}^\perp + (\mathbf{A}_{21} + \gamma^{-1} \mathbf{\Gamma}_{21}) \cdot \mathbf{\Gamma}_{11}^\perp}{|\mathbf{A}_{11} + \mathbf{\Gamma}_{11}| - (1 - \gamma^{-1}) |\mathbf{\Gamma}_{11}|}, \quad (\text{A68})$$

where the orthogonality relation $\mathbf{A}_{12} \mathbf{A}_{11}^\perp = \mathbf{0}$ is taken into account. From Eq. (A68), it can be seen that, by contrast to the transmission matrix (A64a), the reflection matrix is non-singular in the limiting case of thick CLC cells.

We conclude this section with the remark that formulas (A64a) and (A68) are exact and remain applicable outside the photonic band gap.

[1] P. G. de Gennes and J. Prost, *The Physics of Liquid Crystals* (Clarendon Press, Oxford, 1993).

[2] A. B. Harris, R. D. Kamien, and T. C. Lubensky, Rev. Mod. Phys. **71**, 1745 (1999).

[3] H.-S. Kitzerow and C. Bahr, eds., *Chirality in Liquid Crystals*, Partially Ordered Systems (Springer, NY, 2001).

[4] D. W. Berreman and W. R. Heffner, J. Appl. Phys. **52**, 3032 (1981).

[5] Z. L. Xie and H. S. Kwok, J. Appl. Phys. **84**, 77 (1998).

[6] Z. Zhuang, Y. J. Kim, and J. S. Patel, Appl. Phys. Lett. **75**, 3008 (1999).

[7] Z. L. Xie, Y. M. Dong, S. Y. Xu, H. J. Gao, and H. S. Kwok, J. Appl. Phys. **87**, 2673 (2000).

[8] F. S. Y. Fion and H. S. Kwok, Appl. Phys. Lett. **83**, 4291 (2003).

[9] H. Zink and V. A. Belyakov, JETP **85**, 285 (1997).

[10] J. V. Gandhi, X.-D. Mi, and D.-K. Yang, Phys. Rev. E **57**, 6761 (1998).

[11] H. Zink and V. A. Belyakov, Mol. Cryst. Liq. Cryst. **329**, 1069 (1999).

[12] H. G. Yoon, N. W. Roberts, and H. F. Gleeson, Liq. Cryst. **33**, 503 (2006).

[13] V. A. Belyakov and E. I. Kats, JETP **91**, 488 (2000).

[14] V. A. Belyakov, P. Oswald, and E. I. Kats, JETP **96**, 915 (2003).

[15] S. P. Palto, JETP **94**, 260 (2002).

[16] A. D. Kiselev and T. J. Sluckin, Phys. Rev. E **71**, 031704 (2005).

[17] G. McKay, Eur. Phys. J. E **35**, 74 (2012).

[18] I. Lelidis, G. Barbero, and A. L. Alexe-Ionescu, Phys. Rev. E **87**, 022503 (2013).

[19] P. Oswald and P. Pieranski, *Nematic and Cholesteric Liquid Crystals* (Taylor & Francis Group, London, 2005).

[20] V. Vinogradov, A. Khizhnyak, L. Kutulya, Y. Reznikov, and V. Reshetnyak, Mol. Cryst. Liq. Cryst. **192**, 273 (1990).

- [21] S. Kurihara, T. Kanda, T. Nagase, and T. Nonaka, *Appl. Phys. Lett.* **73**, 2081 (1998).
- [22] T. J. White, A. S. Freer, N. V. Tabiryan, and T. J. Bunning, *J. Appl. Phys.* **107**, 073110 (2010).
- [23] T. Kosa, L. Sukhomlinova, L. Su, B. Taheri, T. J. White, and T. J. Bunning, *Nature* **485**, 347 (2012).
- [24] J. P. Vernon, A. D. Zhao, R. Vergara, H. Song, V. P. Tondiglia, T. J. White, N. V. Tabiryan, and T. J. Bunning, *Opt. Express* **21**, 1645 (2013).
- [25] R. Eelkema, *Liq. Cryst.* **38**, 1641 (2011).
- [26] T. N. Orlova and I. P. Terenetskaya, *Opt. Spectrosc.* **100**, 584 (2006).
- [27] I. Terenetskaya and T. Orlova, *Opt. Spectrosc.* **108**, 608 (2010).
- [28] T. N. Orlova and I. P. Terenetskaya, *Mol. Cryst. Liq. Cryst.* **547**, 10 (2011).
- [29] H. J. C. Jacobs and E. Havinga, *Adv. Photochemistry* **11**, 305 (1979).
- [30] J. Saltiel, L. Cires, and A. M. Turek, in *Handbook of Organic Photochemistry and Photobiology*, edited by W. M. Horspool and F. Lenci (CRC Press, London, 2004), chap. 27, pp. 1–22, 2nd ed.
- [31] O. N. Galkin and I. P. Terenetskaya, *J. Photochem. Photobiol. B: Biol.* **53**, 12 (1999).
- [32] M. Born and E. Wolf, *Principles of Optics: Electromagnetic Theory of Propagation, Interference and Diffraction of Light* (Cambridge Univ. Press, New York, 1999), 7th ed.
- [33] R. M. A. Azzam and N. M. Bashara, eds., *Ellipsometry and Polarized Light* (North Holland Publishing Company, Amsterdam, 1977).
- [34] D. Goldstein, *Polarized Light* (Marcel Dekker, NY, 2003), 2nd ed.
- [35] H. G. Tompkins and E. A. Irene, eds., *Handbook of Ellipsometry* (Springer, Berlin, 2005).
- [36] V. A. Belyakov and V. E. Dmitrienko, *Optics of Chiral Liquid Crystals*, vol. 13 of *Soviet scientific reviews* (Harwood Academic Pub., Chur, Switzerland, 1989).
- [37] A. D. Kiselev, R. G. Vovk, R. I. Egorov, and V. G. Chigrinov, *Phys. Rev. A* **78**, 033815 (2008).
- [38] R. I. Egorov, R. G. Vovk, A. D. Kiselev, and M. S. Soskin, in *Proceedings of the XIV-th International Symposium: Advanced Display Technologies* (SID, Ukraine, 2006), pp. 49–53.
- [39] A. D. Kiselev, *J. Phys.: Condens. Matter* **19**, 246102 (2007).
- [40] A. Rapini and M. Papoular, *J. Phys. (Paris) Colloq. C4* **30**, 54 (1969).
- [41] A. D. Kiselev, V. G. Chigrinov, and D. D. Huang, *Phys. Rev. E* **72**, 061703 (2005).
- [42] A. D. Kiselev, E. P. Pozhidaev, V. G. Chigrinov, and H.-S. Kwok, *Phys. Rev. E* **83**, 031703 (2011).
- [43] H. D. Vries, *Acta Crystallographica* **4**, 219 (1951).